







The Identification of a Planar Magnetic Structure within the ICME Shock Sheath and Its influence on Galactic Cosmic-Ray Flux

Zubair I. Shaikh¹ , Anil N. Raghav² , Geeta Vichare¹, Ankush Bhaskar³ , and Wageesh Mishra⁴ 

¹ Indian Institute of Geomagnetism, New Panvel, Navi Mumbai-410218, India; zubairshaikh584@gmail.com

² University Department of Physics, University of Mumbai, Vidyanagari, Santacruz (E), Mumbai-400098, India; raghavani1984@gmail.com

³ Heliophysics Science Division, NASA Goddard Space Flight Center, Greenbelt, MD, USA

⁴ University of Science and Technology of China, People's Republic of China

Received 2018 May 19; revised 2018 August 4; accepted 2018 August 29; published 2018 October 19

Abstract

A Forbush decrease is a sudden decrease in cosmic-ray intensity caused by transient interplanetary disturbances. The substructure of an interplanetary counterpart of a coronal mass ejection (ICME) such as a shock sheath and/or a magnetic cloud independently contributes to cosmic-ray decrease, which is evident as a two-step decrease. Our earlier work has shown multistep decrease and recovery within the ICME-driven shock-sheath region. Further, we have suggested that the presence of a small-scale flux rope within the shock-sheath region causes a steady/gradual recovery in cosmic-ray intensity. Here, we demonstrate the presence of a planar magnetic structure (PMS) and small-scale flux rope within a single shock sheath of an ICME. The plot of the elevation (θ) versus azimuthal (ϕ) angle of the interplanetary magnetic field (IMF) is used for the identification of the PMS. The planarity, efficiency, and a plane-normal vector are estimated by employing a minimum variance analysis (MVA) technique, which confirmed the presence of the PMS. In addition, a 2D-hodogram method in conjunction with the MVA technique is utilized to identify the flux-rope structure and turbulent conditions in the corresponding ICME region. The observation in the visible suggests that the PMS region within the ICME shock sheath caused the decrease in the cosmic-ray flux observed at Earth. It has also been observed that the sharp variations in the IMF (i.e., turbulence) cause a decrease, whereas the flux-rope structure is responsible for the recovery of the CR flux. Further studies are needed to investigate their origins and to confirm their effects on space weather.

Key words: cosmic rays – magnetic fields – solar wind – Sun: coronal mass ejections (CMEs) – turbulence

1. Introduction

Various large-scale solar wind disturbances modulate the omnipresent galactic cosmic rays (GCR) in the heliosphere (Engelbrecht & Burger 2013; Zhao et al. 2014, 2017, 2018; Strauss et al. 2016). The phenomenon of a temporary and rapid decrease in the GCR flux, followed by a comparatively slow recovery lasting for a few days is known as Forbush decreases (FDs; Hess & Demmelmair 1937; Forbush 1938; Lockwood 1971; Cane 2000; Raghav et al. 2017, 2014). This phenomenon was first discovered using ground-based measurements by Forbush (1938) and by Hess & Demmelmair in 1937, and has been extensively studied by many researchers over the last few decades (see, e.g., Lockwood 1971; Cane 2000; Belov et al. 2001; Raghav et al. 2014, 2017; Bhaskar et al. 2016a; Jordan et al. 2011; Dumbovic et al. 2012, and references therein). FDs are generally caused by interplanetary coronal mass ejections (ICMEs) and/or co-rotating interaction regions (CIRs).

Past studies suggest that depending on the intersection of the observer with the substructures of the ICME, i.e., the shock sheath and/or the magnetic cloud (MC), either one-step or two-step FDs are observed (Cane 2000; Richardson & Cane 2010; Raghav et al. 2014). Recently, Raghav et al. (2017) summarized the various distinct features of FDs, such as having (i) a large or small decrease, (ii) a fast or gradual decrease, (iii) a short or long recovery, (iv) a full recovery or

partial recovery or over recovery, (v) one step, two steps, or multiple steps, (vi) a simple or complicated time profile, etc. This might be caused by the vast diversity in the causal solar wind transients, local structures within the structure and their dynamic interactions within the heliosphere. The effect of a local structure within the substructure of ICMEs on the FD profile has been emphasized, and the classical picture of one-step or two-step FDs has been questioned by several groups (Jordan et al. 2011; Raghav et al. 2017; Shaikh et al. 2017). Zhao & Zhang (2016) have also studied two FD events for short-term modulation of GCRs during solar cycle 24 using worldwide neutron monitor stations. Despite their comparable magnitudes, the two Forbush events are distinctly different in terms of the evolving GCR energy spectrum and the energy dependence of the recovery time.

Shaikh et al. (2017) observed a small-scale flux rope within the shock-sheath (assumed to be turbulent) region of the ICME. They demonstrated that these flux ropes contribute to the slow, steady, and gradual recovery of cosmic-ray intensity. Small-scale magnetic flux-rope observations in interplanetary space as well as in the magnetosphere have been reported earlier by many researchers. These small-scale flux ropes have been proposed to have originated from the magnetic reconnection in the local plasma environment (Farrugia et al. 1999; Moldwin et al. 2000; Slavin et al. 2003; Hu et al. 2004, 2014; Cartwright & Moldwin 2008, 2010; Zheng & Hu 2016). The geometry of small-scale flux ropes are similar to that of large-scale flux ropes, i.e., the MCs of ICMEs. However, the size of such flux ropes is very small, ranging from 0.001 to 0.6 au (Moldwin et al. 2000; Feng et al. 2007, 2008). Recently, a new method



Original content from this work may be used under the terms of the [Creative Commons Attribution 3.0 licence](https://creativecommons.org/licenses/by/3.0/). Any further distribution of this work must maintain attribution to the author(s) and the title of the work, journal citation and DOI.

has been developed by Zheng & Hu (2018) to identify small-scale coherent magnetic flux-rope structures in interplanetary space. They identified these structures with durations between 9 and 361 minutes and made a database spanning 20 years for small-scale magnetic flux ropes, using in situ measurement from *Wind* spacecraft data through the GradShafranov reconstruction approach. Here, we have used the MVA and hodogram technique (which is described in Section 2) to identify the type of flux-rope structure in the ICME shock-sheath region. Note that the identification of small-scale flux ropes is less definitive compared to MCs, which have a clear association with ICMEs, originating from the solar corona. Hence, the origin of small-scale flux ropes is still debatable.

Other than small-scale flux ropes, planar magnetic structures (PMSs) are also observed in interplanetary space (Nakagawa et al. 1989). PMSs are distinctive features in the solar wind, characterized by the confinement of interplanetary magnetic field (IMF) vectors to a fixed plane for several hours (Nakagawa et al. 1989; Hakamada 1998). The general properties of PMSs are summarized as follows: (1) the IMF vectors are parallel to one plane and pointing at almost all directions in the same plane, (2) the PMS plane is parallel to the local Archimedean spiral and inclined to the ecliptic plane with a fixed angle, and (3) there is a good relationship between the azimuthal and elevation angles of the IMF. Many studies have been carried out to understand the origin of these structures in the solar wind plasma. They suggest that the PMS originates from the compression of plasma by fast streams (Neugebauer et al. 1993), sector boundary crossings, draping of magnetic field lines about some magnetic structure (Farrugia et al. 1990), and propagation of a fast shock and alignment of pre-existing discontinuities caused by the passage of a shock (Nakagawa 1993; Neugebauer et al. 1993; Jones et al. 1999). The essential criterion for PMS formation in interplanetary space is compression. However, there is no significant correlation between the PMS event and the solar wind speed (Nakagawa 1993). Primarily, there are two large-scale structures in the solar wind where compression occurs frequently: (1) CIRs and (2) the shock-sheath region of ICMEs. Recently, Palmerio (2016) studied in detail the PMSs within the shock-sheath regions of 61 ICMEs. About 80% of the sheaths have a PMS, which are generally observed close to either the CME-driven shock or the MC leading edge, or spanning the whole sheath. The durations of the PMS events range from 1.1 to 18.5 hr, with an average value of 5.3 hr, which is consistent with the previous study by Nakagawa (1993). They also pointed out that events with a high magnetosonic Mach number ($M_A > 2.0$) are more likely to produce a PMS in the immediate shock downstream while quasi-perpendicular shocks produce a PMS close to the MC leading edge (see, e.g., Nakagawa et al. 1989; Jones et al. 1999; Palmerio 2016, and references therein).

In summary, the independent contributions of the shock sheath and MC are considered in the ICME-induced cosmic-ray modulation. Local structures (magnetic flux ropes) are identified within the ICME substructures (i.e., the shock sheath), and their effect on cosmic-ray flux variation has been studied. Recently, unambiguous evidence about the presence of PMS structures within the ICME's shock-sheath region has been reported. The cosmic-ray response to the PMS has not yet been studied. The main aim of our study is to identify the PMS within the shock-sheath region of the ICME and to investigate

its effect on the cosmic-ray variation during the FD phenomena.

2. Data and Methodology

The FD event under study occurred on 2015 December 31. We have used the 92 s time resolution of interplanetary data from the *WIND* database available at https://wind.nasa.gov/mfi_swe_plot.php to study causal ICME structures. We have not considered time shift (which is probably not crucial for the conclusions presented) between the spacecraft and the Earth. We have also used 98 s electron pitch angle distributions from the *WIND*/3D Plasma Analyzer EESA LOW detector available at ftp://cdaweb.gsfc.nasa.gov/pub/data/wind/3dp/3dp_elpd/ for the identification of the boundaries of ICME substructures, i.e., the shock sheath and MC. The cosmic-ray response to the observed ICME is studied using neutron intensity data (with a 10 minute time resolution) from worldwide observatories available at nest.nmdb.eu. To overcome the issues associated with the different baseline and local characteristics, we normalized the neutron flux intensity of each observatory as

$$N_{\text{norm}}(t) = \frac{N(t) - N_{\text{mean}}}{N_{\text{mean}}} \times 100, \quad (1)$$

where N_{mean} is the average of the neutron flux in a specific observatory for a quiet day/days and $N(t)$ is the neutron flux at time t at the same specific observatory. We have categorized the neutron flux data into three energy ranges as follows: (i) low rigidity (0–2 GV), (ii) medium rigidity (2–4.5 GV), and (iii) high rigidity (≥ 4.5 GV). The onset of FDs is characterized by the start of the sharp/gradual decrease in neutron flux, which is done by visual assessment.

2.1. MVA: Method for Identifying Magnetic Flux Ropes

To investigate the presence of different types of magnetic structure and its orientation within the ICME, we have performed Minimum & Maximum Variance Analysis (MVA; see, e.g., Sonnerup & Scheible 1998). After performing MVA, we performed a 2D-hodogram analysis to visualize the geometry of the magnetic structures. Generally, the observation of an arc/semicircular pattern in one of the planes of $B_x - B_y$ or $B_x - B_z$ or $B_z - B_y$ is a good indicator of rotational structure present in interplanetary space and the magnetosphere (Sonnerup & Scheible 1998; Khabarova et al. 2015, 2016; Shaikh et al. 2017). For the MVA analysis, we used high-resolution (11 Hz) IMF data from the *WIND* database, https://wind.nasa.gov/mfi_swe_plot.php. This is used to apply MVA mainly over small regions.

2.2. Method for PMS Identification

The PMS can be considered as a laminar structure, which is composed of sheets that contain parallel but differently oriented magnetic vectors. The main characteristic of the PMS is that the azimuthal (ϕ) and inclination (θ) angles of magnetic field vectors are closely related. When magnetic field vectors, $\mathbf{B} = (B_x, B_y, B_z) \equiv (B \cos \theta \cos \phi, B \cos \theta \sin \phi, B \sin \theta)$, are parallel to a plane whose normal is $\mathbf{n} \equiv (n_x, n_y, n_z)$, the relation between ϕ and θ is given as (Nakagawa et al. 1989;

Nakagawa 1993; Palmerio 2016)

$$n_x \cos \theta \cos \phi + n_y \cos \theta \sin \phi + n_z \sin \theta = 0. \quad (2)$$

The above curve fitting to the measured ϕ and θ distribution in ϕ – θ space indicates the presence of a PMS. The confirmation of the two-dimensionality of the field vectors in PMS events is done using the value of $|B_n|/B$, where B is the magnitude of the IMF and B_n is a component of the magnetic field normal to the PMS plane. Here, B_n is defined as

$$B_n = B \cdot n. \quad (3)$$

The PMS will be a perfect plane when $B_n \approx 0$. Therefore, a low value of $|B_n|/B$ is a good indicator that vectors are almost parallel to a plane (Neugebauer et al. 1993; Palmerio 2016). The value of $B_n/B \leq 0.2$ is considered as the upper limit of the planarity of the PMS in the respective region. A PMS is considered to have a good planarity if $B_n/B \leq 0.1$ (Palmerio 2016).

The magnetic field vectors are almost planar to the PMS plane. Thus, to identify their orientation and the normal, the MVA technique can be employed. The MVA analysis for the selected region will estimate three new directions as the maximum (B_l), intermediate (B_m), and minimum (B_n) variances corresponding to maximum (λ_1), intermediate (λ_2), and minimum (λ_3) eigenvalues and three eigenvectors (\hat{n}_1 , \hat{n}_2 , and, \hat{n}_3), respectively (Sonnerup & Scheible 1998; Palmerio 2016; Shaikh et al. 2017). Here, $\hat{n}_3 \equiv \hat{n}$ represents the normal to the plane. The ratio of intermediate to minimum eigenvalue ($R = \lambda_2/\lambda_3$) gives information about the efficiency of the MVA technique (Nakagawa et al. 1989; Neugebauer et al. 1993; Sonnerup & Scheible 1998). The limit for the eigenvalue ratio is $R \geq 3$.

3. Observations and Interpretations

The studied FD is caused by an ICME that crossed the *Wind* satellite on 2015 December 31st. Figure 1 represents temporal variations of the interplanetary parameters and cosmic-ray intensity. The onset of the shock front is identified as a sudden sharp enhancement in the IMF, solar wind speed, proton temperature, and proton density (shown by the first vertical black dash line). The duration of the ICME-driven shock-sheath region is about ~ 17 hr and 45 minutes. The MC boundaries are shown by the pink vertical dashed lines, where we observe the bidirectional flow of suprathermal electron (see Figure 1), which is also supported by the catalog available at http://space.ustc.edu.cn/dreams/wind_icmes/. The bidirectional flow of electrons within the ICME implies that the ICME is a closed structural loop connected to the Sun at both ends (Shodhan et al. 2000 and references therein). For a detailed investigation, we have divided the complete ICME transit region into different subparts marked as 1–6 as shown in the shaded region in Figure 1, depending on the temporal variations in cosmic-ray intensity. Each subpart corresponds to either a decrease or recovery in cosmic-ray intensity. It is clearly visible that regions 1, 3, and 5 of the shock sheath contribute to cosmic-ray decrease, whereas the regions marked 2 and 6 in the shock sheath lead to a gradual and fast recovery, respectively. During the transit of the leading segment of the MC, the decrease in cosmic-ray intensity is observed, whereas a gradual recovery is observed corresponding to the remaining MC crossover. It implies that the enhanced IMF strength at the

front segment of the MC contributes to the decrease, and the gradual decrease in IMF strength at the trailing segment of the MC is responsible for the gradual recovery in cosmic-ray intensity.

3.1. Region 1

The cyan shaded region in Figure 1 shows the temporal variations of the various solar wind parameters and cosmic rays for region 1. The interplanetary parameters show the sudden enhancement in B_{mag} , V_p , N_p , β , and T_p which can be interpreted as the onset of the shock. The IMF components B_y and B_z show similar temporal variations. The level of the turbulence can be seen from the δB plot as shown in Figure 1. The hodogram analysis (see the first row of Figure 2) also suggests a highly turbulent structure. Corresponding to this turbulent structure (lowest panel in Figure 1), we observe a decrease in cosmic-ray flux, in all energy bands, of about 2% as compared to the flux in the pre-shock region.

3.2. Region 2

A gradual increase in B_T with large fluctuations (see the δB plot shown in Figure 1) is observed in region 2. The plasma temperature T_p shows an increase while N_p shows a little decrease as compared to region 1. The IMF components B_x , B_y , and B_z as well as θ and ϕ show high fluctuations. Moreover, the hodogram in the x – z plane shows fluctuations having a curved structure, which indicates a disturbed flux-rope-like structure (see the second row of Figure 2). It may be a consequence of the plasma relaxation process in the turbulent shock-sheath region (Taylor 1986). The cosmic ray shows a very slow and gradual recovery during the passage of this substructure.

3.3. Region 3

The total IMF is high at about 14 nT and shows constant and steady variations in region 3. However, the sharp decrease is observed in B_y and B_z . The hodogram corresponding to this region does not reveal any structural information. The sharp variations in the IMF components are responsible for the scattering, and a high magnetic field shields the particles from diffusion; therefore, these might be the reasons for the decrease in cosmic-ray flux (see Figure 1).

3.4. Region 4

In Figure 2 (see the fourth row corresponding to region 4), we can clearly observe an arc/semicircular-like structures in the x – z plane, which clearly depict a flux-rope structure. We also confirm the presence of flux-rope-type structures in this region from the database provided by the Zheng & Hu (2018). In this region, we observe a fast recovery/increase in cosmic-ray flux in all energy bands (see the bottom panel of Figure 1). To justify that the increase in cosmic-ray intensity is not associated with a ground-level enhancement (GLE) event, we analyzed *GOES* spacecraft's X-ray and proton flux data. There was no solar energetic proton (SEP) event associated with the aforementioned cosmic-ray intensity increase. Therefore, we do not expect any GLE signature during the passage of the ICME. This explicitly indicates that the enhancement is not associated with the GLE event. We observe a small decrease in the total IMF and solar wind speed. The solar wind proton density and plasma beta remain almost constant, while the plasma

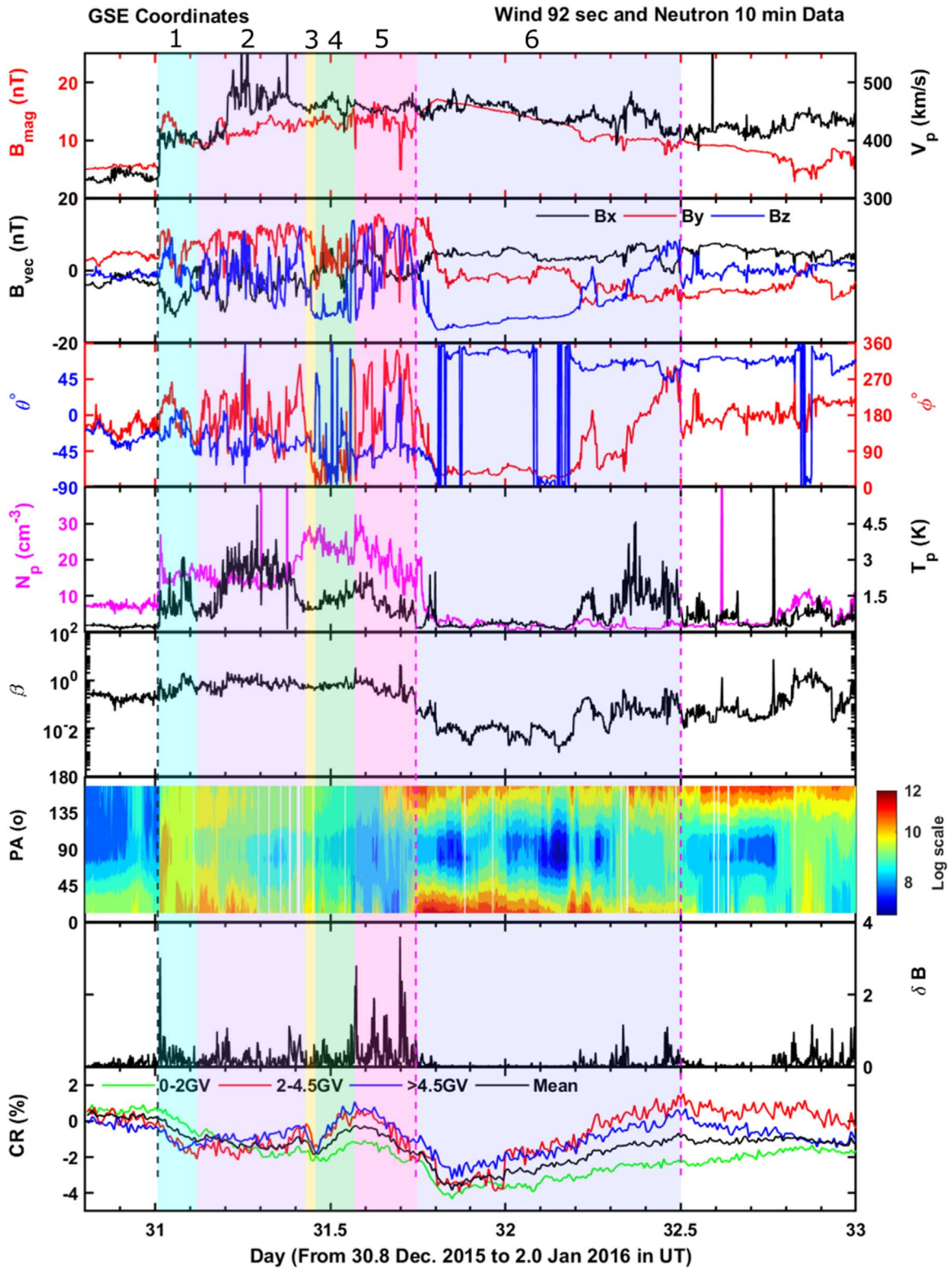


Figure 1. Forbush decrease event that occurred on 2015 December 31. It has eight panels; the topmost panel shows the temporal variation of the IMF B_{mag} and V_p . The second and third panels represent the components of the interplanetary magnetic field, B_x , B_y , and B_z , and the azimuth (ϕ) and elevation angles (θ) of the magnetic field vector. The fourth panel shows the plasma density (N_p) and temperature ($T_p = \times 10^3$ K). The fifth panel represents the plasma beta (β). Further, panels six and seven describe the electron (164.96 eV) pitch angle ($(s^3 \text{ cm}^{-6})$) distribution and the standard deviation of the IMF as δB (nT). The δB is calculated as $\delta B_i = \frac{B_{i+1} - B_{i-1}}{2}$. The subsequent panel, the sixth, shows the normalized neutron flux with its respective band of rigidities. The sudden shocks that commence are shown by vertical black dashed lines, while MC boundaries are shown with pink vertical dashed lines. The five different regions of the shock sheath and MC are separated by differently colored shades. The rigidity of the cosmic-ray flux ranges from 0–2, 2–4.5, and >4.5, corresponding to the energy ranges 0–1.270, 1.270–3.658, and >3.658 GeV respectively (Shea 2001).

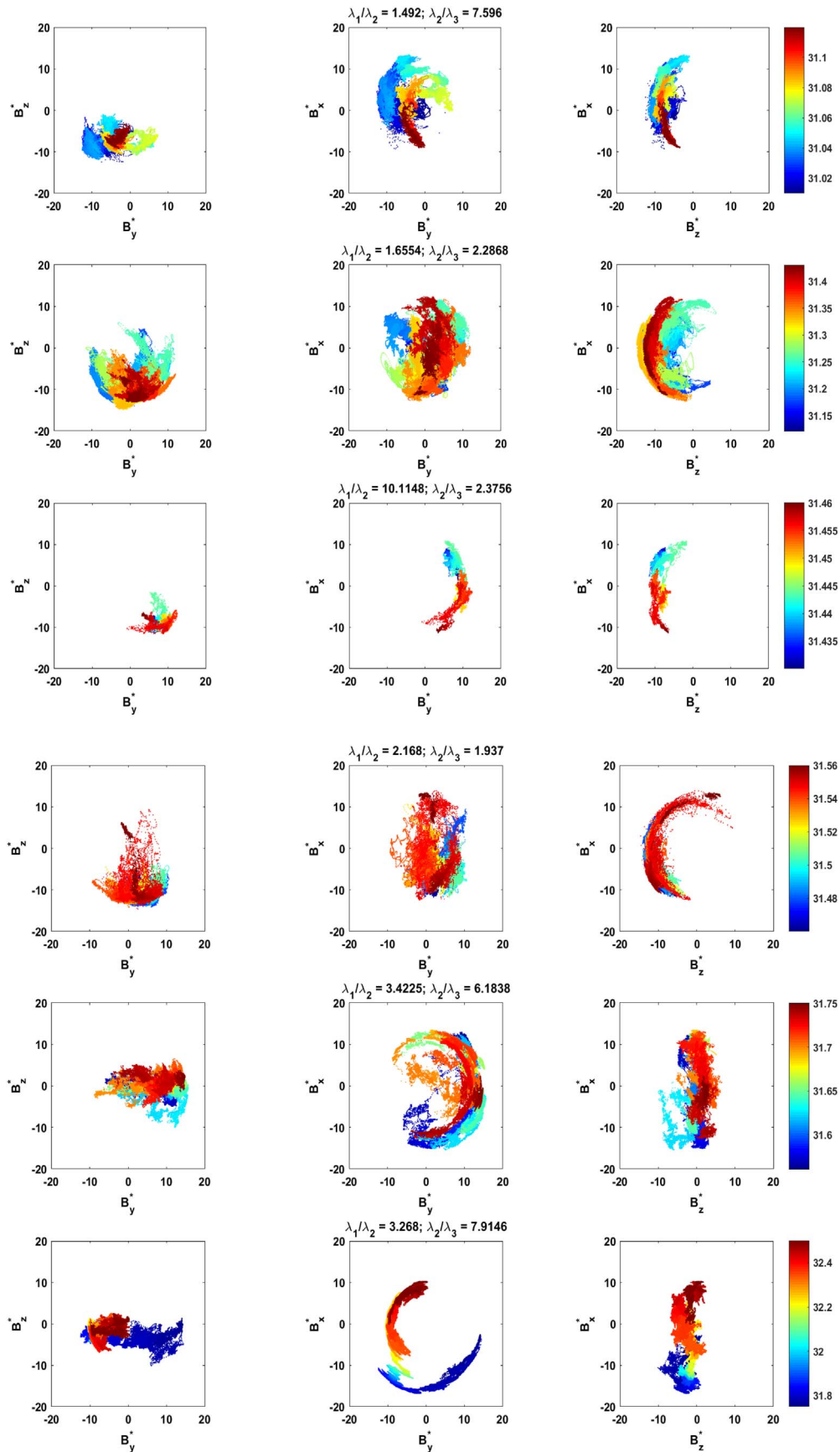


Figure 2. Hodogram plot of the different subregions. Each row represents the hodogram of the different regions (i.e., from regions 1 to 6) in a different plane of projections. B_x^* , B_y^* , and B_z^* (corresponding to maximum (λ_1), intermediate (λ_2), and minimum (λ_3) eigenvalues) are the magnetic field vectors after MVA analysis. The corresponding ratio of the eigenvalues is added for each region. Regions 1–5 belong to the shock sheath of the ICME, and region 6 represents the magnetic cloud.

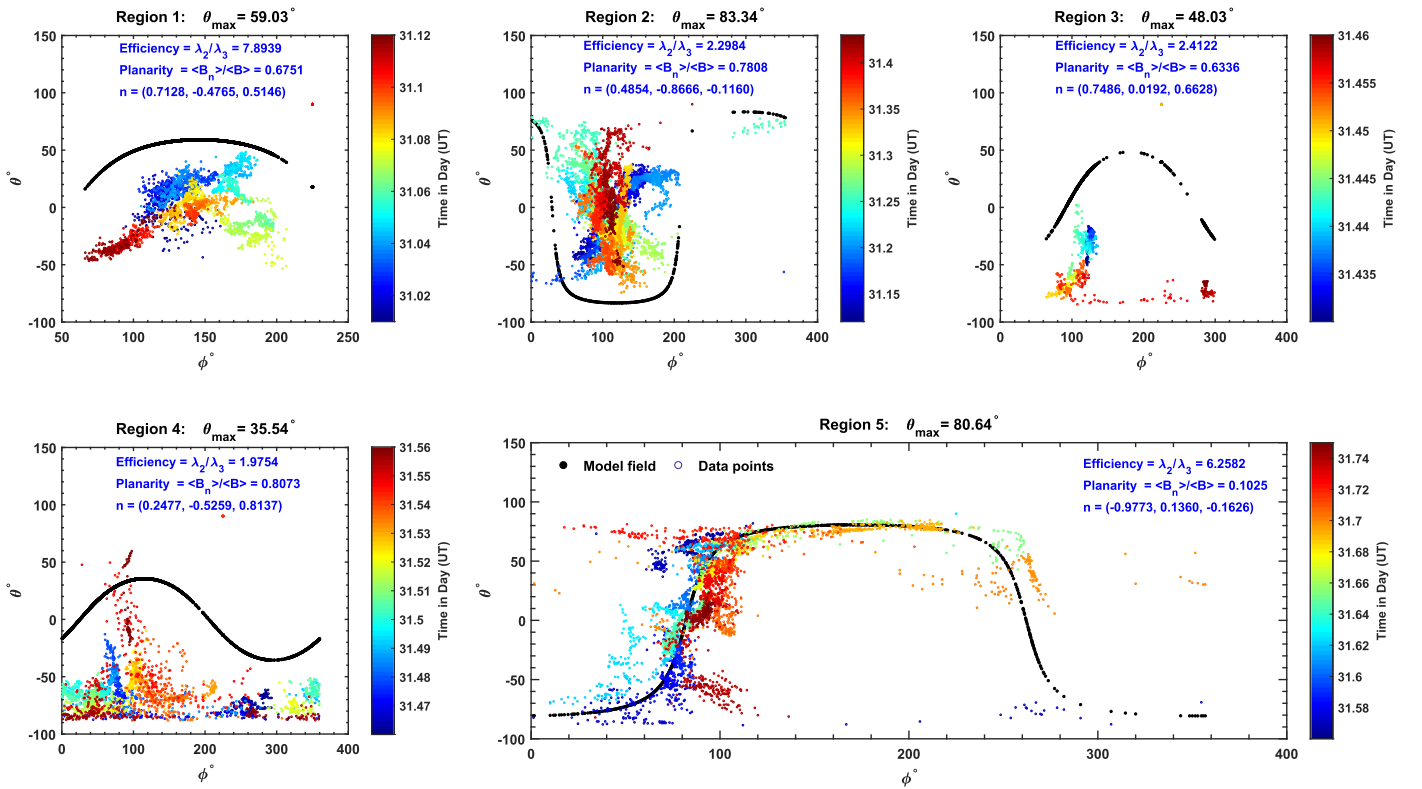


Figure 3. The ϕ – θ distribution for regions 1–5 within the ICME-driven shock-sheath region (see the regions in Figure 1). ϕ is the azimuthal angle of the magnetic field vector, and θ is the angle of the field vector from the ecliptic plane. The angular distribution of the model field vectors corresponding to the observations is shown by the black curve. The temporal variations of the ϕ – θ distribution for the given regions are shown by color bars. We observe only one PMS structure, which is at the trailing edge of the ICME’s shock sheath (i.e., region 5). In the PMS plane, the IMF vectors are parallel and contains the spiral direction (i.e., at $\theta = 0^\circ$, we get $\sim\phi = 82^\circ.45$ and $\sim\phi = 262^\circ.10$). The inclination of the PMS plane to the ecliptic plane is given by θ_{\max} . For this, *WIND* satellite data of 3 s time resolution is utilized.

temperature increases gradually. The fluctuation (δB) associated with this region is also low compared to regions 1 and 2, as expected for ordered structures within the turbulent shock-sheath region. Thus, the ordered structure (flux rope) with decreasing magnetic field causes the recovery in cosmic-ray intensity.

3.5. Region 5

Region 5 spans the period of about 4 hr and 33 minutes. The average solar wind speed in this region is about 450 km s^{-1} . The estimated thickness of region 5 is about ~ 0.05 au. The interplanetary parameters N_p , T_p , and β within this region show a gradual decrease. The total IMF (B_T) and all its components display high fluctuations, while the plasma speed remains almost steady. We observe that the turbulence in this region is very high compared to that in regions 1–4 (see the seventh panel in Figure 1), which may be due to more compression present at the front of the MC. The arc-like structure with distortion is visible in the x – y plane of the hodogram as shown in the fifth row of Figure 2. A structure is said to be planar if the following criteria are satisfied: (1) a wide distribution of the ϕ angle, $0^\circ < \phi < 360^\circ$, (2) good planarity, i.e., $B_n/B \leq 0.2$, and (3) good efficiency $R = \frac{\lambda_2}{\lambda_3} \geq 3$ (Nakagawa et al. 1989; Palmerio 2016). The PMS analysis reveals that region 5 is a good PMS. The corresponding θ and ϕ distribution is shown in Figure 3. The efficiency (λ_2/λ_3) and planarity ($\langle B_n \rangle / \langle B \rangle$) of this region are 6.2585 and 0.1025, respectively. The PMS plane is inclined to the ecliptic plane by angle $\theta_{\max} = 80^\circ.64$. At $\theta = 0$, the PMS structure tends to intersect at about $\phi = 82^\circ.45$

and $\phi = 262^\circ.10$, i.e., the Archimedean spiral direction is also included in the plane. The vector normal to this PMS plane is the eigenvector corresponding to the minimum eigenvalue, which is $n = (-0.9773, 0.1360, -0.1626)$. Figure 3 shows the best model fitting (see Equation(2)) for this region. Thus, region 5 satisfies all the criteria necessary for a region to be a PMS. It is also observed that there is a decrease in cosmic-ray intensity during the transit of the PMS.

3.6. Region 6

This region belongs to the MC of the ICME. The region starts from day 31.75 to 32.5 in UT (i.e., about 18 hr). During this period, the average plasma speed is about 450 km s^{-1} ; therefore, the thickness of this region (i.e., the MC) is about 0.2 au. We notice a gradual decrease in total IMF and almost steady variation in plasma speed with small fluctuation. The interplanetary parameters N_p , T_p , and β remain low except at the trailing edge where we observe a heating effect. The δB remains very low as compared to regions 1–5 during this transition region, which shows that region 6 is fluctuating less, as expected for ordered structures i.e., the flux-rope structure. The IMF components B_y and B_z remain negative throughout the region except at the front edge, where we observe a sudden transition from west to east for B_y , and from north to south for B_z . B_x increases and remains positive and steady during this region. Therefore, we will observe a clear rotational structure in the x – y plane after MVA (see the hodogram plot as shown in the sixth row of Figure 2). It is noticed that during the transit of the MC, the cosmic-ray flux decreases initially to its lowest

value and then gradually recovers to its ambient value. The decrease in cosmic-ray flux may be due to the enhanced IMF field strength, while the recovery is due to a decrease in the IMF B_T within the ordered structure of the MC.

4. Discussion and Conclusion

FD is generally understood in terms of physical processes such as diffusion, convection, and turbulence associated with ICME substructures and CIRs. The classical picture of ICME-induced FD suggests a two-step decrease in which the first step is caused by the shock sheath and the second is caused by the MC (Cane 2000; Richardson & Cane 2011; Raghav et al. 2014). Recently, Raghav et al. (2017) proposed a new classification scheme for FDs and introduced multistep complex FD events. In general, it is understood that the ICME-driven shock sheath is turbulent (Joe & Jokipii 2007) and contributed to the decrease in cosmic-ray flux (Cane 2000; Subramanian et al. 2009; Babu et al. 2013; Raghav et al. 2014). Recently, Shaikh et al. (2017) observed an ordered structure (flux rope) within the shock sheath of the ICME, which can contribute to the recovery of cosmic-ray flux. In fact, what types of local structures are formed or are present within the shock-sheath region of the ICME is an open problem. Shaikh et al. (2017) confirmed a small-scale flux rope, while Palmerio (2016) affirmed a PMS structure in the shock-sheath region of the ICME. The present models are incapable of explaining the observed complex multistep profile of FDs. It is still not known and needs to be found which part of the shock sheath contributes to the step/gradual decrease and/or in the recovery of cosmic-ray flux, as well as the reason behind it. Here, in this study, we identify the PMS within the shock-sheath region and attempt to investigate its effect on cosmic-ray variations.

Regions marked 1, 3, and 5 and the leading part of region 6 as in Figure 1 show decreases in cosmic-ray intensity. The sudden sharp variations in the IMF vector components might be responsible for the decrease in cosmic-ray intensity during the crossovers of regions 1 and 3. The small amplitude variations in the total IMF and its components are seen in region 2, which could explain the steady variation in cosmic-ray intensity. The arc/semicircular pattern in the x - z plane visible in the hodogram as shown in Figure 2 corresponding to region 4 indicates the possible existence of a small-scale flux-rope structure. It is possible that the local ordered structure may present/evolve in the shock-sheath region due to the plasma relaxation process and/or magnetic islands in the turbulent post-shock fluid due to shock waves and/or the dynamics of magnetic island reconnection and turbulent processes (Taylor 1986; Joe & Jokipii 2007; Greco et al. 2010; Karimabadi et al. 2014; Zank et al. 2015). The presence of 2D magnetic islands or vortex structures in nearly incompressible magnetohydrodynamics (NI MHD) plasma having $\beta \sim 1$ or $\ll 1$ is predicted by Zank & Matthaeus (1992, 1993), Bieber et al. (1996), and Zank et al. (2017). The size of the magnetic islands varies from an hour to minutes to ion kinetic scales (Khabarova et al. 2015, 2016; Lion et al. 2016, and references therein). At the ion kinetic scale, the β of the solar wind embedded with vortex/magnetic island structures is < 1 . The trapped charged particles in a merging or contracting magnetic island might gain higher energy due to stochastic reflection from boundaries of the closed magnetic field line structures or interaction with the reconnection electric field of the island. Evidences of particle acceleration (from the keV to MeV energy range) are observed

at various places in interplanetary space (the places where the magnetic islands are observed; Cartwright & Moldwin 2008, 2010; Gosling et al. 2010; Zank et al. 2014, 2015; Khabarova et al. 2015, 2016; Le Roux et al. 2015, 2016). Further, Zank et al. (2014) and Le Roux et al. (2015) proposed theoretical models for the propagation of charged particles in a “sea” of magnetic islands. However, whether this physical mechanism contributes to cosmic-ray acceleration processes is the fundamental question. The sharp recovery observed in region 4 may be associated with the aforementioned acceleration mechanism. However, the developed model only supports the acceleration of particles having energy in the keV to MeV range, and GeV particles are outside the purview of the above discussed model. Therefore, at this moment, it is difficult to conclude about the similar acceleration mechanism for the CR particles as discussed in (Raghav & Shaikh 2016) and further studies in this direction are needed. Here, in this studied event, we observed the gradual recovery corresponding to the observed small-scale flux rope, which is in agreement with the earlier study of Shaikh et al. (2017). Similarly, the front edge of the MC with the enhanced IMF strength and sharp variations in the IMF vector components probably lead to the cosmic-ray decrease in region 6. However, the recovery of the cosmic-ray intensity is visible during the crossover of the trailing segment of the MC. The gradual decrease in magnetic field strength might be the reason behind the gradual recovery in cosmic-ray intensity.

Besides this, the detailed analysis of region 5 reveals that the planar magnetic structure is presented at the trailing edge of the shock sheath (see Figures 1 and 3). We observe that the angle ϕ has a distribution from 0° to 360° , i.e., the complete range, the planarity of the region is 0.1025, and the efficiency is 6.2585. Further, region 5 shows the best fitting model as given by Equation (2) (see the bottom-right subplot in Figure 3). All the above-said criteria suggest that the region 5 shows a distinct PMS structure. We have also calculated the thickness of the PMS by taking the complete duration of the region and average wind speed corresponding to the same region. The estimated thickness of region 5 is 1.23×10^5 km. The inclination (θ_{\max}) of the above PMS with respect to that of ecliptic plane is 80.64° . The observed PMS may have originated from the amplification and alignment of pre-existing discontinuities in the ambient solar wind compressed by the ICMEs. The compression by lateral expansion of ICMEs may cause the alignment of the discontinuities in the vicinity of the HCS (Neugebauer et al. 1993). The study suggests that PMS neither originates in the solar wind nor during flares or filaments eruption (Nakagawa 1993). PMS has been observed at different occasions like: in the vicinity of the sector boundary, in the center of a sector, recurrently at the same heliospheric longitude in successive rotations of the Sun (Nakagawa 1993). These studies suggest that the source of a PMS is on the Sun (Nakagawa 1993; Neugebauer et al. 1993). It might happen that due to compression of the shock sheath in the leading and trailing edges, a PMS develops in the shock-sheath region of the studied event.

The identified PMS within this event in region 5 shows that the magnetosonic Mach number (M_{ms}) and Alfvénic Mach number M_A is about ~ 6 and ~ 7.5 , respectively. The earlier statistical study gives the upper limit of M_{ms} and M_A within the PMS structures observed in the 2 hr downstream region of the shock as $M_{\text{ms}} > 2.5$ (Palmerio 2016) and $M_A > 2$ (Kataoka

et al. 2005), respectively. Further, Kataoka et al. (2005) argued that the PMS will be absent in the shock downstream when $M_A < 2$ and the $\beta < 0.05$. From the Figure 1, we can observe that the average β within region 5 is about ~ 0.5 , i.e., plasma beta > 0.05 . Therefore, our analysis of PMS is in agreement with that of previously reported parameters. Moreover, the high Mach number within region 5 implies that the presence of PMSs in the trailing edge of the shock sheath can be associated with the high ion densities and high magnetic field magnitudes at the beginning of the MC. The increased ion density can be correlated with the compressed regions in the vicinity of the sheath's trailing edge, called the piled-up compression region.





The gradual decrease in cosmic-ray intensity is clearly evident to correspond to the PMS transit in Figure 1. We observe from δB in Figure 1 that the magnetic field within region 5 is more turbulent compared to the other regions of the shock sheath. In general, the magnetic field components are normal to those of the background average magnetic field. Therefore, if the gyroradii of the particles are small compared to that of the largest scales in the turbulent plasma (magnetic field), then particle motion along the field line contributes to the perpendicular motion. This phenomenon is known as the effect of the field line random walk. This random walk contributes to the diffusion of particles because particles move along the randomly varying components of the magnetic field normal to the background field, i.e., the angle between the field component and mean field determines the motion of the particle normal to the average field. A planar region having compressed fluid in the direction about normal to the average magnetic field increases the magnetic field component normal to the flow (or parallel to that of the average magnetic field). But the compression will not change the field component perpendicular to the average field. Further, these processes decrease the angle between the field components and average magnetic field, which results in a reduction of field line random walk and hence perpendicular diffusion occurs. Therefore, we observe a step decrease in particle transport across the magnetic field in a given planar region. (Intriligator & Siscoe 1995; Intriligator et al. 2001). Similarly, in our analysis, we observed the PMS in the trailing edge of the ICME shock sheath, which is highly compressed due to the compression by the MC of the ICME. Therefore, the compression may be the origin of the PMS at the trailing edge of shock sheath. This compression may decrease the perpendicular diffusion and the random walk of field lines. Therefore, this may contribute to the step decrease in cosmic-ray flux during the PMS (region 5) transit. The shock barrier model proposed by Wibberenz et al. (1998) may be employed to understand the decrease in cosmic-ray intensity corresponding to PMS transit. Further detailed study is needed in this direction to understand the cosmic-ray response to the PMS.

In summary, our study explicitly shows that the PMS and flux-rope structures may develop/be present within a single shock-sheath region (considered to be turbulent) of the ICME. The sharp variations in the total IMF and its components, as well as the PMS structures, contribute to the decrease in cosmic-ray intensity, while that of the ordered flux-rope structure is responsible for the recovery. The study also asserts that local structures such as flux ropes and PMSs within the ICME-driven shock-sheath region are very important to the investigation of cosmic-ray modulation/variations. A detailed study is needed to understand the origin of the flux rope and

PMS within the shock-sheath region of the ICME. Further, it is also important to find out whether PMSs always cause a decrease, or do they cause recovery? Therefore, a study with rigorous statistical analysis is needed to understand the influence of PMSs and the underlying physical process responsible for the cosmic-ray modulation.

We acknowledge the NMDB database (www.nmdb.eu) founded under the European Union's FP7 programme (contract No. 213007). We are also thankful to all neutron monitor observatories listed on the website. We are thankful to CDAWeb and the WIND database for making interplanetary data available. We are also thankful to the University of Science and Technology of China (USTC) for providing the ICME catalog. We are thankful to Miss Gauri Datar for helping us with the preparation of the manuscript. We heartily thank the Indian Institute of Geomagnetism and Department of Physics, the University of Mumbai for providing us with facilities for the fulfillment of this work. We thank the anonymous reviewer who help us to improve this article. We thank to the editorial office of the Astrophysical Journal for editing this manuscript.

ORCID iDs

Zubair I. Shaikh  <https://orcid.org/0000-0002-9206-6327>
 Anil N. Raghav  <https://orcid.org/0000-0002-4704-6706>
 Ankush Bhaskar  <https://orcid.org/0000-0003-4281-1744>
 Wageesh Mishra  <https://orcid.org/0000-0003-2740-2280>

References

- Babu, A., Antia, H. N., Dugad, S. R., et al. 2013, *A&A*, **555**, A139
 Battarbee, M., Dalla, S., & Marsh, M. S. 2017, *ApJ*, **836**, 138
 Belov, A., Eroshenko, E., Oleneva, V., Struminsky, A., & Yanke, V. 2001, *AdSpR*, **27**, 625
 Belov, A. V. 2008, in IAU Symp. 257, Universal Heliophysical Processes, ed. N. Gopalswamy & D. F. Webb (Cambridge: Cambridge Univ. Press), 439
 Bhaskar, A., Prasad, S., & Vichare, G. 2016b, *ApJ*, **828**, 104
 Bhaskar, A., Vichare, G., Arunbabu, K. P., & Raghav, A. 2016a, *Ap&SS*, **361**, 242
 Bieber, J. W., Wanner, W., & Matthaeus, W. H. 1996, *JGR*, **101**, 2511
 Bothmer, V., & Rust, D. M. 1997, in Coronal Mass Ejections, ed. N. Crooker, J. A. Joselyn, & J. Feynman (Washington, DC: AGU), 139
 Burlaga, L., Sittler, E., Mariani, F., & Schwenn, R. 1981, *JGR*, **86**, 6673
 Cane, H. V. 2000, *SSRv*, **93**, 55
 Cartwright, M. L., & Moldwin, M. B. 2008, *JGRA*, **113**, A09105
 Cartwright, M. L., & Moldwin, M. B. 2010, *JGRA*, **115**, A08102
 Drake, J. F., Swisdak, M., Che, H., & Shay, M. A. 2006, *Natur*, **443**, 553
 Dumbovic, M., Vrsnak, B., Calogovic, J., & Zupan, R. 2012, *A&A*, **538**, 28
 Engelbrecht, N. E., & Burger, R. A. 2013, *ApJ*, **779**, 158
 Farrugia, C. J., Dunlop, M. W., Geurts, F., et al. 1990, *GeoRL*, **17**, 1025
 Farrugia, C. J., Janoo, L. A., Torbert, R. B., et al. 1999, in AIP Conf. Proc. 471, Solar Wind Nine, ed. G. A. Gary & S. F. Nerney (Melville, NY: AIP), 745
 Feng, H. Q., Wu, D. J., & Chao, J. K. 2007, *JGRA*, **112**, A02102
 Feng, H. Q., Wu, D. J., Lin, C. C., et al. 2008, *JGRA*, **113**, A12105
 Forbush, S. E. 1938, *PhRv*, **54**, 975
 Gosling, J. T., Teh, W. L., & Eriksson, S. 2010, *ApJL*, **719**, L36
 Greco, A., Servidio, S., Matthaeus, W. H., & Dmitruk, P. 2010, *P&SS*, **58**, 1895
 Hakamada, K. 1998, *SoPh*, **181**, 73
 Hess, V. F., & Demmelmair, A. 1937, *Natur*, **140**, 316
 Hu, Q., Qiu, J., Dasgupta, B., Khare, A., & Webb, G. M. 2014, *ApJ*, **793**, 53
 Hu, Q., Smith, C. W., Ness, N. F., & Skoug, R. M. 2004, *JGRA*, **109**, A03102
 Intriligator, D. S., Jokipii, J. R., Horbury, T. S., et al. 2001, *JGR*, **106**, 10625
 Intriligator, D. S., & Siscoe, G. L. 1995, *JGR*, **100**, 21605
 Joe, G., & Jokipii, J. R. 2007, *ApJL*, **663.1**, L41
 Jones, G. H., Balogh, A., & Horbury, T. S. 1999, *GeoRL*, **26**, 13
 Jordan, A. P., Spence, H. E., Blake, J. B., & Shaul, D. N. A. 2011, *JGRA*, **116**, A11103
 Karimabadi, H., Roytershteyn, V., Vu, H. X., et al. 2014, *PhPl*, **21**, 062308

- Kataoka, R., Watari, S., Shimada, N., Shimazu, H., & Marubashi, K. 2005, *GeoRL*, **32**, L12103
- Khabarova, O., Zank, G. P., Li, G., et al. 2015, *ApJ*, **808**, 181
- Khabarova, O. V., & Zank, G. P. 2017, *ApJ*, **843**, 4
- Khabarova, O. V., Zank, G. P., Li, G., et al. 2016, *ApJ*, **827**, 122
- Le Roux, J. A., Zank, G. P., Webb, G. M., & Khabarova, O. 2015, *ApJ*, **801**, 112
- Le Roux, J. A., Zank, G. P., Webb, G. M., & Khabarova, O. V. 2016, *ApJ*, **827**, 47
- Lepping, R. P., Burlaga, L. F., Tsurutani, B. T., et al. 1991, *JGR*, **96**, 9425
- Lion, S., Alexandrova, O., & Zaslavsky, A. 2016, *ApJ*, **824**, 47
- Lockwood, J. A. 1971, *SSRv*, **12**, 658
- Low, B. C. 2001, *JGR*, **106**, 25141
- Marubashi, K., Akiyama, S., Yashiro, S., et al. 2015, *SoPh*, **290**, 1371
- Moldwin, M. B., Ford, S., Lepping, R., Slavin, J., & Szabo, A. 2000, *GeoRL*, **27**, 57
- Nakagawa, T. 1993, *SoPh*, **147**, 169
- Nakagawa, T., Nishida, A., & Saito, T. 1989, *JGR*, **94**, 11761
- Neugebauer, M., Clay, D. R., & Gosling, J. T. 1993, *JGR*, **98**, 9383
- Palmerio, E. 2016, *AnGeo*, **34**, 313
- Raghav, A., Bhaskar, A., Lotekar, A., Vichare, G., & Yadav, V. 2014, *JCAP*, **10**, 074
- Raghav, A., & Shaikh, Z. 2016, arXiv:1610.09628
- Raghav, A., Shaikh, Z., Bhaskar, A., Datar, G., & Vichare, G. 2017, *SoPh*, **292**, 99
- Richardson, I. G., & Cane, H. V. 2010, *SoPh*, **264**, 189
- Richardson, I. G., & Cane, H. V. 2011, *SoPh*, **270**, 609
- Shaikh, Z., Raghav, A., & Bhaskar, A. 2017, *ApJ*, **844**, 121
- Shea, M. A. 2001, in *Advances in Space Research* (New York: Elsevier), 1773
- Shodhan, S., Crooker, N. U., Kahler, S. W., et al. 2000, *JGR*, **105**, 27261
- Slavin, J. A., Lepping, R. P., Gjerloev, J., et al. 2003, *JGRA*, **108**, 1015
- Sonnerup, B. U., & Scheible, M. 1998, in *Analysis Methods for Multi-Spacecraft Data*, ed. G. Paschmann & P. Daly (Noordwijk: ESA), 185
- Strauss, R. D., le Roux, J. A., Engelbrecht, N. E., Ruffolo, D., & Dunzlaff, P. 2016, *ApJ*, **825**, 43
- Subramanian, P., Antia, H. M., Dugad, S. R., et al. 2009, *A&A*, **494**, 1107
- Taylor, J. B. 1986, *RvMP*, **58**, 741
- Wibberenz, G., Le Roux, J. A., Potgieter, M. S., & Bieber, J. W. 1998, *SSRv*, **83**, 309
- Zank, G. P., Adhikari, L., Hunana, P., et al. 2017, *ApJ*, **835**, 147
- Zank, G. P., Hunana, P., Mostafavi, P., et al. 2015, *ApJ*, **814**, 137
- Zank, G. P., Le Roux, J. A., Webb, G. M., Dosch, A., & Khabarova, O. 2014, *ApJ*, **797**, 28
- Zank, G. P., & Matthaeus, W. H. 1992, *JGR*, **97**, 17189
- Zank, G. P., & Matthaeus, W. H. 1993, *PhFIA*, **5**, 257
- Zhao, L. L., Adhikari, L., Zank, G. P., Hu, Q., & Feng, X. S. 2017, *ApJ*, **849**, 88
- Zhao, L. L., Adhikari, L., Zank, G. P., Hu, Q., & Feng, X. S. 2018, *ApJ*, **856**, 94
- Zhao, L. L., Qin, G., Zhang, M., & Heber, B. 2014, *JGRA*, **119**, 1493
- Zhao, L. L., & Zhang, H. 2016, *ApJ*, **827**, 13
- Zheng, J., & Hu, Q. 2016, *JPhCS*, **767**, 012028
- Zheng, J., & Hu, Q. 2018, *ApJL*, **852**, L23
- Zurbuchen, T. H., & Richardson, I. G. 2006, in *Coronal Mass Ejections*, ed. H. Kunow et al. (New York: Springer), 31